iScience

CellPress
OPEN ACCESS

Article

Factors influencing initial bacterial adhesion to antifouling surfaces studied by single-cell force spectroscopy

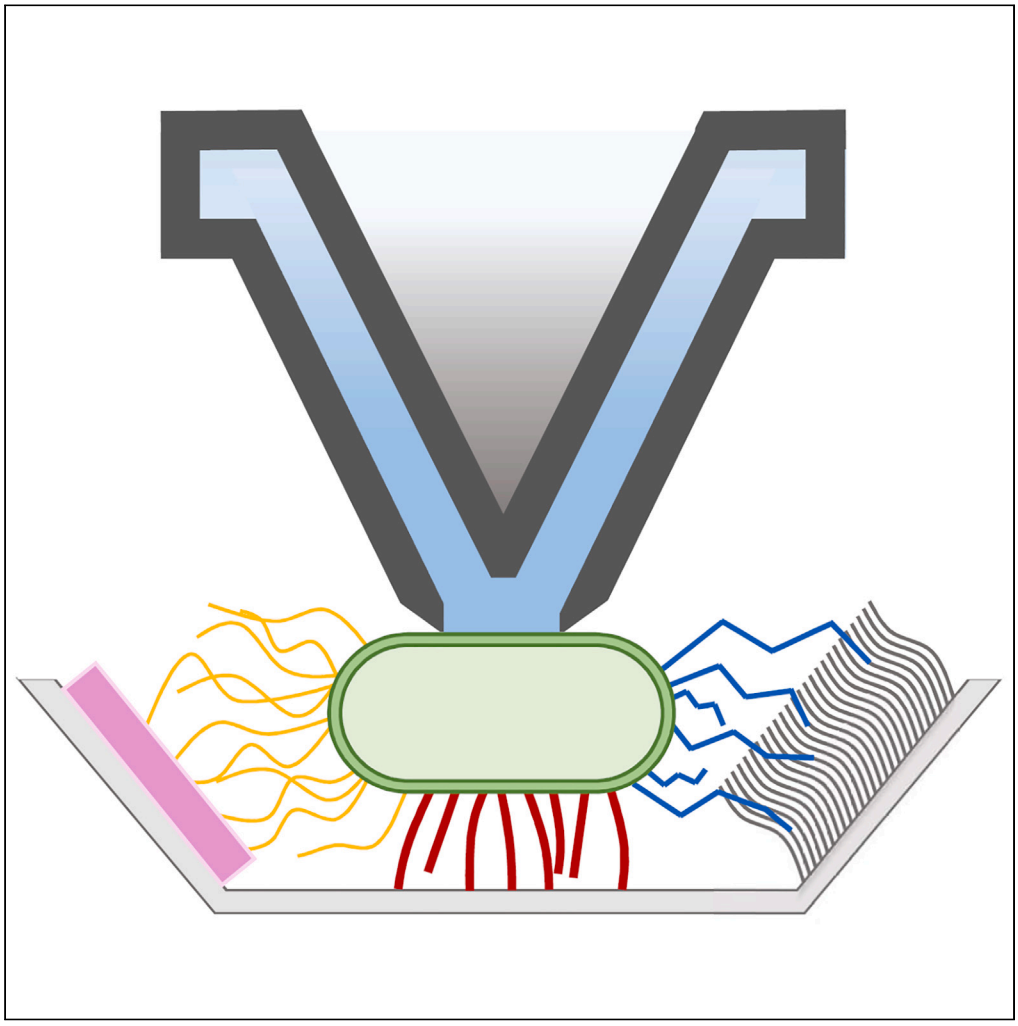

Tal Duanis-Assaf, Meital Reches

meital.reches@mail.huji.ac.il

Highlights

Research at the single-cell level can enhance our understanding of bacterial adhesion

E. coli adheres to different antifoulants via separate mechanisms

The peptide prevents the initial adhesion of *E. coli* as the antifouling polymer brush PEG

Duanis-Assaf & Reches, iScience *27*, 108803
February 16, 2024
https://doi.org/10.1016/j.isci.2024.108803

iScience

CellPress
OPEN ACCESS

Article

Factors influencing initial bacterial adhesion to antifouling surfaces studied by single-cell force spectroscopy

Tal Duanis-Assaf[1] and Meital Reches[1,2,*]

SUMMARY

Biofilm formation, a major concern for healthcare systems, is initiated when bacteria adhere to surfaces. *Escherichia coli* adhesion is mediated by appendages, including type-1 fimbriae and curli amyloid fibers. Antifouling surfaces prevent the adhesion of bacteria to combat biofilm formation. Here, we used single-cell force-spectroscopy to study the interaction between *E. coli* and glass or two antifouling surfaces: the tripeptide DOPA-Phe(4F)-Phe(4F)-OMe and poly(ethylene glycol) polymer-brush. Our results indicate that both antifoulants significantly deter *E. coli* initial adhesion. By using two mutant strains expressing no type-1 fimbriae or curli amyloids, we studied the adhesion mechanism. Our results suggest that the bacteria adhere to different antifoulants via separate mechanisms. Finally, we show that some bacteria adhere much better than others, illustrating how the variability of bacterial cultures affects biofilm formation. Our results emphasize how additional study at the single-cell level can enhance our understanding of bacterial adhesion, thus leading to novel antifouling technologies.

INTRODUCTION

Bacterial biofilms are communities of bacteria that adhere to surfaces and to each other.[1] In biofilm, bacteria engulf themselves with an extracellular matrix composed of polysaccharides, proteins, and nucleic acids.[2] It is believed that the extracellular matrix protects against environmental threats such as antibiotics, antimicrobials, and toxins.[2] Therefore, biofilms are a major concern in the food and medical industries, as well as in water and healthcare systems.[3] Hospital-acquired infections are caused by antibiotic-resistant strains. One of the most common hospital-acquired infections is catheter-associated urinary tract infection (CAUTI). Many CAUTI cases are caused by pathogenic *Escherichia coli* strains, which form biofilm on the surface of the catheter.[4]

The complex process of biofilm formation is typically initiated by the adhesion of bacteria to abiotic surfaces. This is followed by bacteria adhering to each other and secreting components of the extracellular matrix.[5] The matrix further promotes the adhesive nature of the biofilm, thus increasing its stability and supporting biofilm growth.[6]

The attachment of *E. coli* to abiotic surfaces is reinforced by extracellular appendages.[5] These non-flagellar proteinaceous filaments may expose specific adhesins and may play multiple roles.[7] Type 1 fimbriae (or pili) feature the FimH adhesin, which specifically binds to mannose as a colonization strategy of epithelial cells.[8,9] However, these organelles were also shown to be essential for adhesion to abiotic surfaces.[10,11] The *fimA* gene encodes the main repeating unit of type 1 fimbriae, and the knockout mutations of that gene prevent type 1 fimbriae expression.[12] Curli amyloid fibers were also shown to be associated with biofilm formation.[13] These filaments, also termed thin aggregative fimbriae, promote adhesion to abiotic surfaces as well as cell aggregation.[14,15] The CsgA protein serves as the main repeating subunit of curli amyloid, facilitating fiber formation.[16]

In recent years, various approaches to prevent biofilm formation have been developed. Owing to the difficulty of removing mature biofilms, it is especially desirable to prevent the formation of biofilm before it is initiated. One approach uses novel antifouling surface coatings that reduce the accumulated biomass.[17] Some of the most promising coatings include polymer brushes,[18–20] slippery liquid-infused porous surface (SLIPS),[21–23] and anti-adhesive assemblies of peptides and peptoids.[24–27]

One of the best methods of quantitatively measuring cell adhesion is single-cell force spectroscopy (SCFS)[28] using atomic force microscopy (AFM).[29] In recent years SCFS has emerged as a powerful method for studying the initial bacterial attachment. Sullan, Beaussart[30] studied the colonization mechanism of epithelial cells by *Lactobacillus rhamnosus* bacteria and revealed that the bacteria pili interact either via nanospring or nanotether mechanisms. Khan, Aslan[31] investigated the recognition of fibronectin by *Staphylococcus epidermidis* and determined that it specifically binds to the fibrillar protein structure. Lafont and collaborators[32] examined the interaction between *Yersinia*

[1]Institute of Chemistry and The Center for Nanoscience and Nanotechnology, The Hebrew University of Jerusalem, Jerusalem 91904, Israel
[2]Lead contact
*Correspondence: meital.reches@mail.huji.ac.il
https://doi.org/10.1016/j.isci.2024.108803

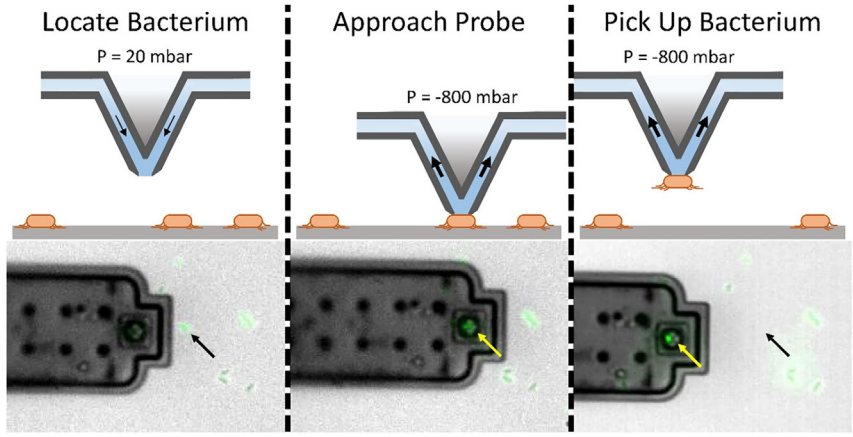

Figure 1. A schematic representation of the sequence of steps leading to the bacterial immobilization on the FluidFM probe (top) and the optical visualization of the different stages (bottom)

The optical microscopy images consist of brightfield overlaid with fluorescent images of the bacteria labeled with SYTO 9. The immobilization sequence consists of locating a proper bacterium (left), aligning the probe on top of the target cell, approaching it (middle), and applying negative pressure to pick up the bacterium (right). The black arrows denote the original position of the target bacterium, and the yellow arrows denote the position of the target cell after aspiration.

pseudotuberculosis and solid surfaces and observed significantly weaker interactions with substrates coated with polymer brushes. Recent studies used SCFS to show a correlation between the initial attachment of different bacteria and their ability to form a biofilm.[33,34]

The fluidic force microscope (FluidFM) combines traditional AFM with a pressure controller and a hollow cantilever to form a force-controlled micropipette.[35] This apparatus was recently used to conduct SCFS measurements with bacterial cells.[36,37] These studies demonstrated the improved throughput allowed by FluidFM, moreover, it was shown that results obtained by FluidFM are consistent with those obtained by traditional AFM.[37] Potthoff, Ossola[36] were able to measure the detachment forces of a chain of *Streptococcus pyogenes* from the substrate. They observed a sawtooth pattern as the bacterial chain was detached in a cell-by-cell manner, showing that these bacteria attached to each other better than to the surface. Hofherr, Müller-Renno[37] were able to conduct SCFS measurements with the bacterium *Lactococcus lactis*, which was previously unreliable due to difficulties in immobilization by traditional adhesive based methods.

Here, we employ SCFS using a FluidFM to study the initial adhesion of *E. coli* to bare glass, and glass coated with an antifouling peptide (AFP) layer or poly(L-lysine) grafted with poly(ethylene glycol) (PLL*g*PEG). Our results show the efficiency of both antifoulants to deter *E. coli* initial attachment. Furthermore, we observed that *E. coli* can utilize different appendages to adhere to different surfaces and that the adhesion to the various antifoulants is mediated by different mechanisms. Finally, we demonstrate that adhesion is also influenced by the variability of the bacterial cells.

RESULTS

Our goal was to determine the factors that affect the initial attachment of bacteria to different antifouling surfaces. We focused on surface coatings that rely on self-assembled thin transparent layers and that require simple fabrication procedures. We chose a commercially available PLL*g*PEG as a model for antifouling polymer, since PEG brushes are considered the "gold standard" of antifouling coatings.[38] The short AFP DOPA-Phe(4F)-Phe(4F)-OMe[39] was chosen as a model for antiadhesive peptide-based coating because it is a simple molecule that is easy to apply. *E. coli* was chosen as a model biofilm-forming organism due to its relevance to healthcare systems, as well as the available knowledge regarding the different adhesion factors utilized by this bacterium to adhere to abiotic surfaces. We used FluidFM to perform SCFS and study the interactions between *E. coli* and bare glass (positive control), AFP, and PLL*g*PEG during the initial adhesion. Using this method, we aimed to better understand the mechanism underlying bacterial initial attachment to different surfaces.

The surfaces were characterized using water contact angle measurements (Table S1) and energy-dispersive X-ray spectroscopy (EDS; Figure S1; Table S2). The AFP surface showed a characteristic increase in the contact angle due to the addition of a hydrophobic peptide coating.[39] PLL*g*PEG-coated glass also showed an increase in the contact angle; these results for PLL*g*PEG are similar to previously reported values.[40] For both antifouling surfaces, the signal of the carbon increased when compared with bare glass. The carbon signal slightly increased for glass coated with an AFP layer and was more strongly elevated for glass coated with PLL*g*PEG brushes. The difference in carbon content on the coated surfaces indicates the presence of the organic coating layer.

Each SCFS experiment consisted of several stages. First, a cell probe was prepared by immobilizing a single bacterium on the tip (Figure 1). Second, the cell probe was used for interaction measurements. Third, the bacterium was released from the probe by applying high positive pressure (1000 mbar), and the whole cycle was repeated. Figure 1 shows a schematic representation of the sequence of steps leading to the immobilization of the bacterium, alongside optical microscopy images of each step. The bright field images are overlaid with fluorescent images of the bacteria labeled with SYTO 9. The FluidFM cantilever was placed above a single bacterium and approached while applying a negative pressure to aspirate the cell. The probe was then retracted and moved aside to determine whether the cell was immobilized on

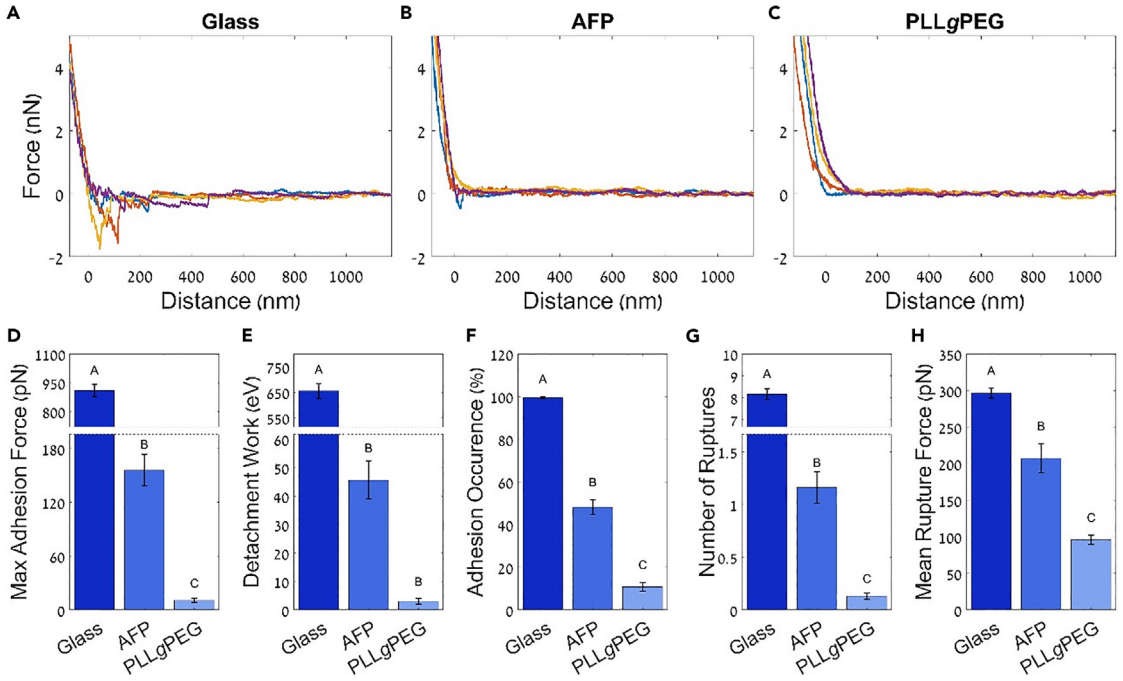

Figure 2. Interactions measured by SCFS for the *E. coli* WT strain with bare glass and glass coated with either AFP or PLL*g*PEG

The top panel shows typical force profiles against the bare glass (A), AFP (B), and PLL*g*PEG (C), featuring four representative force curves. The bottom panel shows summary data for the maximum adhesion force (D), detachment work (E), adhesion occurrence as the percentage of curves featuring adhesion events (F), the mean number of rupture events per curve (G), and the mean force measured for single rupture events (H). Data are represented as the mean ± standard error. The different letters represent significantly different groups as determined by one-way ANOVA followed by a post hoc Bonferroni test ($p < 0.05$).

the FluidFM tip. After successful bacterium immobilization, the cell probe was used to measure the interaction with the substrate. The experimental cycle is schematically shown in Figure S2. In short, the cell probe approached the substrate, followed by a short pause, to allow the bacterium to interact with the surface. Then, it was retracted from the surface, until full detachment was achieved.

Typical force curves obtained for the adhesion of *E. coli* ATCC 25922 strain (WT) to bare glass, AFP, and PLL*g*PEG are shown in Figures 2A–2C. For bare glass, multiple detachment events were typically observed, featuring an overall adhesion force in the nN regime. The average value of the measured maximum adhesion force was 910 ± 30 pN, and the average detachment work was 660 ± 30 eV (Figures 2D and 2E). The multiple rupture events can generally be explained by multiple binding moieties, such as fimbriae and adhesins.[41–44] Force plateaus may also appear, largely due to membrane tethering and pili extension.[45,46] Interestingly, the interaction between a different *E. coli* strain (DSM 429) and bare glass was previously shown to be substantially weaker.[34] These measurements were carried out at a lower set point, which may result in a lower contact area, and thus a decreased adhesion.[36] Nevertheless, they show that two strains of the same species can have a distinct adhesion force. The force profiles for either AFP or PLL*g*PEG showed a notable difference from those of glass, with fewer adhesion events and a lower overall adhesion force. This is also confirmed by the summary data, with an average maximum adhesion force of 160 ± 20 pN for AFP and 10 ± 2 pN for PLL*g*PEG, and a mean detachment work of 46 ± 7 eV for AFP and 3 ± 1 eV for PLL*g*PEG. These average values do not represent actual rupture forces measured at the 10 pN regime, but rather are the result of including in the average value many curves which feature no detectable adhesion, as observed in the typical force profiles (Figure 2C). The maximum adhesion force for such curves, is counted as 0 pN. Both measurements are significantly smaller for both antifoulants compared with glass (Figures 2D and 2E).

The adhesion occurrence (Figure 2F) was calculated as the proportion of force curves featuring any measurable adhesion (in percentage). This measurement shows that the bacteria adhered to bare glass almost in all the measurements, with an adhesion occurrence of ~100%; however, the adhesion occurrence was significantly reduced to 48 ± 3% for AFP and 11 ± 2% for PLL*g*PEG. This suggests that the probability of bacterial initial attachment is significantly lower for both antifouling surfaces. It is worth mentioning that the reduced adhesion occurrence affects the calculated overall adhesion force and the detachment work, since measurements that featured no adhesion were still added to the average calculation as 0 pN, and 0 eV, respectively. Therefore, studying individual rupture events can enhance our understanding of specific adhesion events during the initial attachment of *E. coli* to different surfaces.

When bacteria have multiple anchoring sites to the surface, the attachment is stronger. Thus, the mean number of rupture events per curve is a good indication of the attachment strength. The mean number of adhesion events per measurement was calculated as 8.2 ± 0.2, 1.2 ± 0.1, and 0.13 ± 0.03 for bare glass, AFP, and PLL*g*PEG, respectively (Figure 2G). By analyzing the individual interaction forces, we observed mean rupture forces of 296 ± 7 pN, 210 ± 20 pN, and 96 ± 6 pN for bare glass, AFP, and PLL*g*PEG, respectively (Figure 2H). Both measurements were significantly lower for the AFP surface and were further reduced for PLL*g*PEG. These results show that both antifouling surfaces

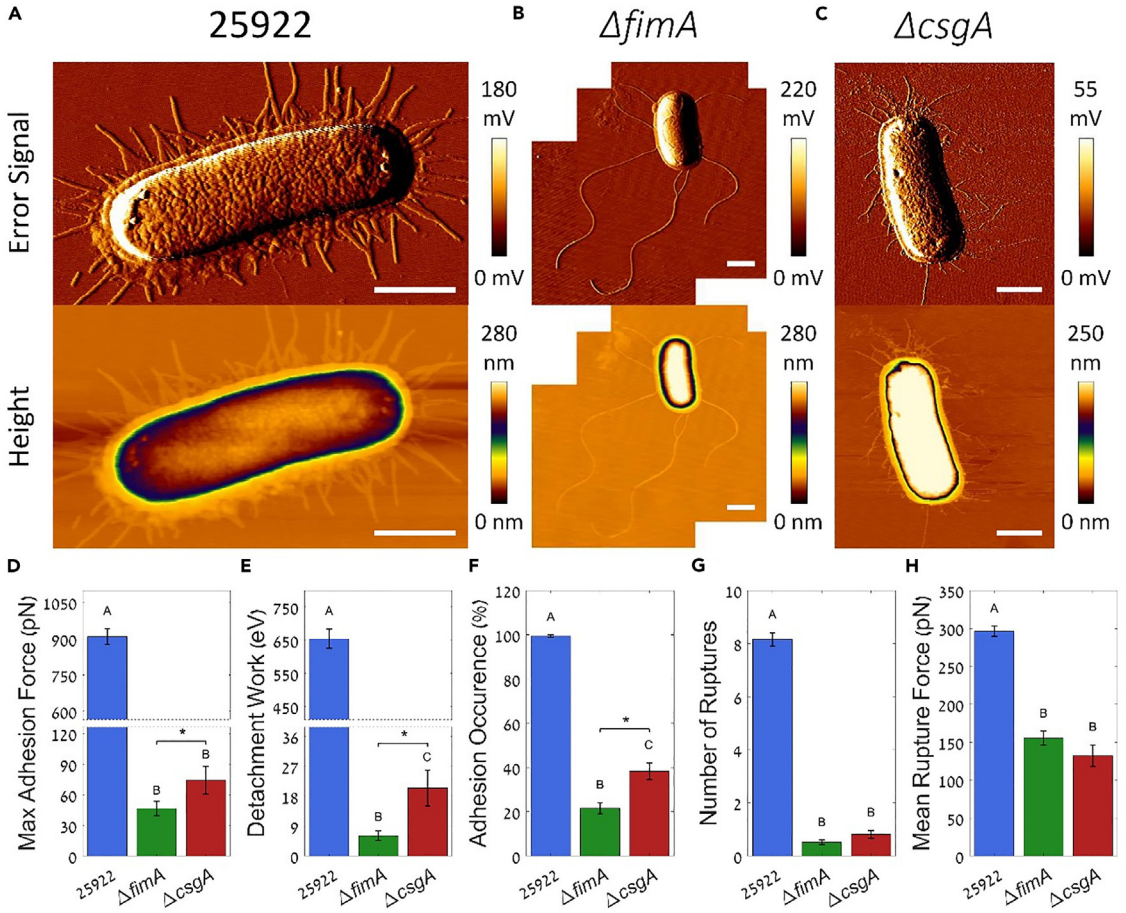

Figure 3. Contribution of different appendages to the adhesion of *E. coli* to glass

(A–C) Representative AFM images showing the error signal and the measured height of single *E. coli* cells of the WT (A), ΔfimA (B), and ΔcsgA (C) strains. The images were taken on mica under dry conditions. The scale bars correspond to 1 μm. The image in (B) consists of three separately acquired images to capture the whole cell with the flagella. The bottom panel shows a comparison between the adhesion measured by SCFS between the different strains and a bare glass, displaying summary data for the maximum adhesion force (D), detachment work (E), adhesion occurrence as the percentage of curves featuring adhesion events (F), the mean number of rupture events per curve (G), and the mean force measured for single rupture events (H). Data are represented as the mean ± standard error. The different letters and asterisks represent significantly different groups as determined by one-way ANOVA, followed by a post hoc Bonferroni test or a t test, respectively ($p < 0.05$).

significantly impair the *E. coli* initial attachment. Moreover, according to these observations, even when adhesion does occur, it is significantly weaker, and hence, poses less of a threat, since bacteria are probably removed more easily.

Note that during the experimental setup, we washed the substrate to remove non-adherent cells so that they do not interfere while aspirating the cells to prepare the single-cell probe. Apart from suspended cells, many of the weakly bound cells are also removed during this step. This means that our measurements are initially performed on the more adhesive cells. Thus, the adhesion we measured is probably augmented compared with the original cell culture. In the traditional method, cells must be well adhered to the substrate during aspiration. Otherwise, they are prone to slide horizontally when a force is applied, and the preparation of the cell probe will probably fail. Therefore, measurements by FluidFM are possibly less biased toward high adhesion than using the traditional method.

Another point to keep in mind is that when performing repeated measurements with the same bacterium there is a concern of introducing bias due to interaction between the cell surface and the substrate. To minimize this effect, we added a pause at the end of each measurement cycle (force curve) of a few seconds, to allow the cell to stabilize before interacting with the surface again. We could not observe a specific trend in any of the adhesion metrics (max adhesion force, detachment work, number of rupture events, and mean rupture force) over the consecutive measurement with the single-cell probes. We therefore assume that repeated force measurements with a single bacterium did not introduce significant positive nor negative bias to adhesion.

To determine how different appendages contribute to bacterial adhesion ability, we compared the 25922 strain (WT) to two *E. coli* K12 mutant strains from the Keio collection[47]: (i) *ΔfimA*, not expressing type 1 fimbriae and (ii) *ΔcsgA*, not expressing curli amyloid fibers. Both appendages were previously shown to be associated with bacterial adhesion to abiotic surfaces.[11,48] Representative AFM images of single bacteria from these three strains are shown in Figure 3.

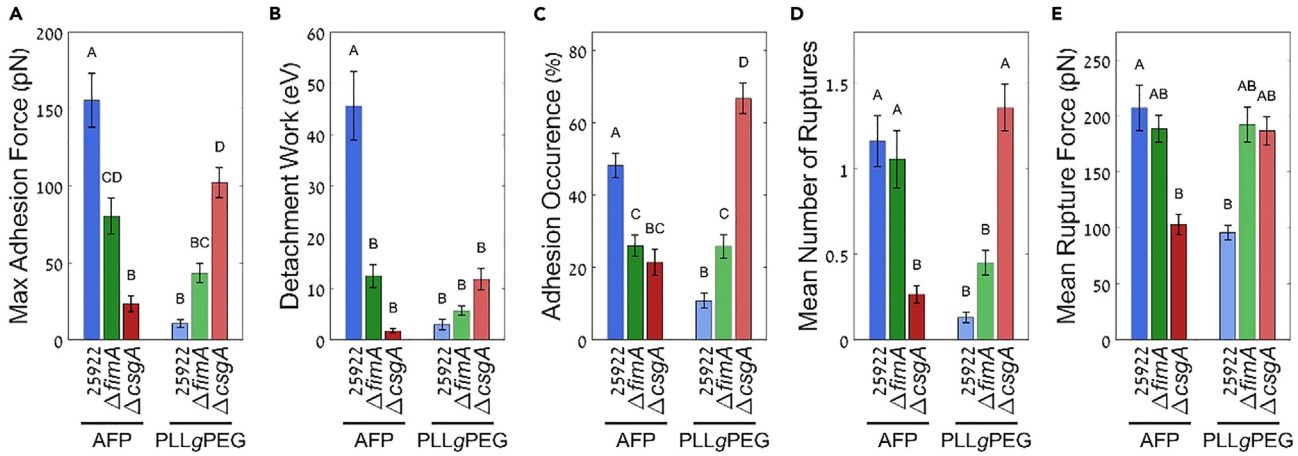

Figure 4. Comparison of the adhesion of the WT, ΔfimA, and ΔcsgA strains to glass surfaces coated with either AFP or PLLgPEG by SCFS

Summary data are presented for the maximum adhesion force (A), detachment work (B), adhesion occurrence as the percentage of measurements featuring adhesion events (C), the mean number of rupture events per force curve (D), and the mean rupture force measured for single events (E). Data are represented as the mean ± standard error. The different letters represent significantly different groups as determined by one-way ANOVA, followed by a post hoc Bonferroni test ($p < 0.05$).

The adhesion of both mutant strains to glass was measured using SCFS, and a summary comparing these results to the WT strain is shown in Figures 3D–3H. Although both strains had significantly weaker adhesion to glass compared with the WT, *ΔfimA* had a much lower max adhesion force, detachment work, and adhesion occurrence compared with *ΔcsgA*, with a difference of ∼40%, ∼70%, and ∼43%, respectively, but had similar values for the number of rupture events per measurement and the mean rupture force. The detachment work and the adhesion occurrence also showed a statistically significant difference according to ANOVA and the Bonferroni test. Furthermore, by performing individual statistical comparisons using a t test,[49] the max adhesion force was also significantly different. This suggests that type 1 fimbriae contribute to the initial adhesion to bare glass more than curli amyloids do.

Wong, Olsson[50] observed similar results using total internal reflection fluorescence (TIRF). They reported that adhesion by the *ΔfimA* strain is weaker than for both the native K-12 and the *ΔcsgA* mutant strains. Intriguingly, their results indicated a higher adhesion occurrence for *ΔfimA*, which they attributed to repulsion induced by appendages. Our finding that *ΔfimA* had the lowest adhesion occurrence seems to contradict their results. However, in our experimental setup, the bacteria are brought in contact with the surface by the forces exerted by the AFM probe, which most likely increases the probability of adhesion, by overcoming the weak repulsion imposed by bacterial fimbriae. Potthoff, Ossola[36] have also shown that by increasing the force applied by the AFM, the adhesion was intensified in correlation with the force. Taken together, our results as well as others'[11,50,51] show that type 1 fimbriae play a major role during the *E. coli* initial attachment to bare glass.

The adhesion of the three strains to both AFP and PLL*g*PEG was compared (Figure 4). For the AFP surface, we observed that the maximum adhesion force was significantly higher for the WT, compared with both mutant strains. The maximum adhesion force was 80 ± 10 pN and 23 ± 5 pN for *ΔfimA* and *ΔcsgA*, respectively, amounting to a decrease of 50% and ∼85% in the measured force for *ΔfimA* and *ΔcsgA*, compared with the WT. The detachment work followed the same trend, featuring a significant decrease for *ΔfimA* and *ΔcsgA*, compared with the WT, where the energy was found to be lower by 75% and 95%, respectively (12 ± 2 eV and 1.7 ± 0.4 eV, respectively). Moreover, *ΔfimA* had a significantly higher adhesion force and a much higher detachment work than *ΔcsgA*.

The adhesion occurrence of the WT was significantly higher (almost double) than both *ΔfimA* and *ΔcsgA*; however, there was no appreciable difference between the two mutants, which were calculated as 25 ± 3% and 21 ± 4%, respectively. The number of rupture events per force curve was comparable for the WT and *ΔfimA*, and slightly lower for ΔcsgA; all were calculated at fewer than two rupture events per curve, on average. Finally, the mean rupture force was similar for WT and *ΔfimA*, but much lower for *ΔcsgA*, with an average of 180 ± 10 pN for *ΔfimA* and 102 ± 9 pN for *ΔcsgA*. It is worth mentioning again that the maximum adhesion force average value is greatly affected by curves featuring no adhesion, whereas the mean rupture force is strictly calculated by the measured adhesion events, completely disregarding curves that do not feature adhesion. This explains how the maximal adhesion force can be lower than the mean rupture force, especially due to the low adhesion occurrence shown here.

All the adhesion metrics reported previously indicate that the WT strain has a higher adhesive propensity to AFP than both mutant strains, which is followed by *ΔfimA*; *ΔcsgA* adheres to AFP with the least potency. These results suggest that curli amyloids, which are absent in the *ΔcsgA* strain, may contribute more to the interaction with the AFP surface. A possible explanation for this observation could be the formation of π-π interactions between the aromatic peptide and the aromatic residues on the protein, which facilitate the assembly of amyloid fibers.[52,53]

This trend changes, however, when analyzing the interaction between the bacterium and PLL*g*PEG. Here, the WT has weakened interactions. Although most measurements did not show a significant difference between the WT and *ΔfimA*, they did have a slightly higher maximal

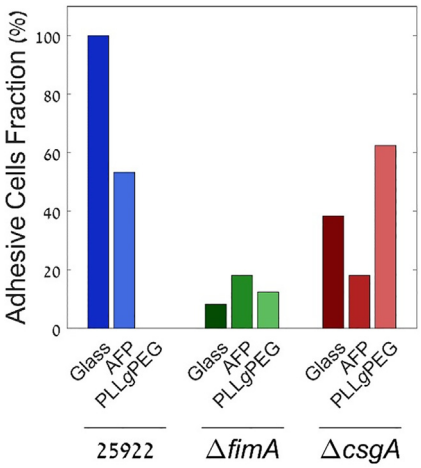

Figure 5. A qualitative analysis of adhesive cells for each strain and surface

Bacteria are counted here as adhesive if they have measurable adhesion in at least 50% of the curves (for that specific cell). Data are presented as the percentage of adhesive cells for each strain-substrate pair in percentage.

adhesion force and detachment work, and a significantly higher adhesion occurrence (more than double). Surprisingly, *ΔcsgA* did adhere better to PLL*g*PEG than did the WT. The max adhesion force for *ΔcsgA* was 100 ± 10 pN, which was approximately 90% higher than that of the WT. *ΔcsgA* had a significantly higher adhesion force than *ΔfimA*, which was less than half (43 ± 6 pN). The detachment work of *ΔcsgA* was higher as well; the calculated values of 12 ± 2 eV was roughly 75% higher than that of the WT, and double that of *ΔfimA* (6 ± 1 eV). The mean rupture force was almost the same for both mutant strains, with roughly 190 pN, a much higher value than the rupture force of the WT (96 ± 6 pN). However, the most prominent change was the adhesion occurrence, which were 67 ± 4% for *ΔcsgA* and 26 ± 3 for *ΔfimA*. Less striking was the number of rupture events per measurement, which was fewer than 2 for all strains, and it was highly affected by the adhesion occurrence.

These results indicate that the *ΔcsgA* strain adheres much better to PLL*g*PEG than do the other two strains. They also suggest that neither type 1 fimbriae nor curli amyloids play a significant role in the adhesion mechanism when the surface is PLL*g*PEG. It is therefore likely that this attachment is more affected by other physical interactions, rather than proteinaceous appendages. Zeng, Ogaki[54] have shown that *Staphylococcus epidermidis* can utilize extracellular DNA and polysaccharides to adhere to PEGylated Ti surfaces. Moreover, the antifouling mechanism of PEG polymer brushes is generally attributed to their strong hydration.[17,38,55] Therefore, changes in the cell hydrophilicity may affect the short-term attachment to PEGylated surfaces. Indeed, it was previously shown that *ΔcsgA* is more hydrophilic than the WT.[48] Hence, it is possible that the stronger adhesion to PLL*g*PEG observed for *ΔcsgA* results from other adhesion factors, not related to fimbrial appendages.

Bacterial cultures are inherently variable in many of their bacterial traits. Therefore, information about single cells can be very valuable.[56] One of the most important benefits of using SCFS is the ability to determine the adhesive nature of a single bacterium. Using data acquired for single cells, we can differentiate between highly adhesive cells and cells with low adhesion to the surface. One possibility is to rely on the differences in adhesion occurrence on a per-cell basis. Figure 5 shows the percentage of adhesive cells for each strain-substrate pair, where each cell is considered adhesive if it possesses measurable adhesion in at least 50% of the measurements.

According to this characterization, 100% of the WT cells adhered to bare glass, but only 53% adhered to AFP, and 0% adhered to PLL*g*PEG. *ΔfimA* had less than 20% adhesive cells for all substrates. AFP had slightly more adhesive cells (18%) than did PLL*g*PEG (12.5%), and bare glass had the least (8.3%). *ΔcsgA* had better adhesiveness to bare glass compared with *ΔfimA*, with 38% adhesive cells, and had the same percentage of adherent cells to AFP (18%). Interestingly, *ΔcsgA* had the highest percentage of adhesive cells to PLL*g*PEG (62.5%) compared with the other strains, supporting the results described previously.

This analysis can be performed more quantitatively by investigating the specific adhesion events for each bacterium. We chose to focus on the number of adhesion events and the measured rupture forces as an indication of good adhesion, and we determined the maximal values calculated for each cell, since we believe that it best represents the potential of each cell to adhere to the surface. These data are shown in Figure 6 as histograms of the bacteria count over the maximal number of rupture events and the maximal observed rupture force.

The results show that all WT cells had relatively strong adhesion to glass, whereas almost all *ΔfimA* cells had much weaker adhesion. However, several *ΔcsgA* cells had adhesion comparable to that of the WT. On AFP we observed that most WT cells had much weaker adhesion compared with glass. However, a number of cells still had adhesion as strong as the WT strain had to bare glass. In comparison, all *ΔcsgA* cells had relatively weak adhesion to AFP. On PLL*g*PEG, almost all WT cells had weak adhesion compared with glass: only one cell had a number of rupture events similar to those of glass, but no rupture forces were above 200 pN. The *ΔcsgA* strain showed stronger adhesion in more than half of the cells.

These results indicate that the antifouling surfaces successfully reduce the adhesion strength of most cells. However, some of the cells have a better adhesive capacity, which enables them to adhere eventually. Over time, these surface-bound bacteria can affect the surface chemistry of the substrate by secreting extracellular matrix components and other reactive species. Consequently, this can create a favorable environment and promote further bacterial adhesion, and eventually the formation of biofilm, which may seriously challenge the existing antifouling technology.

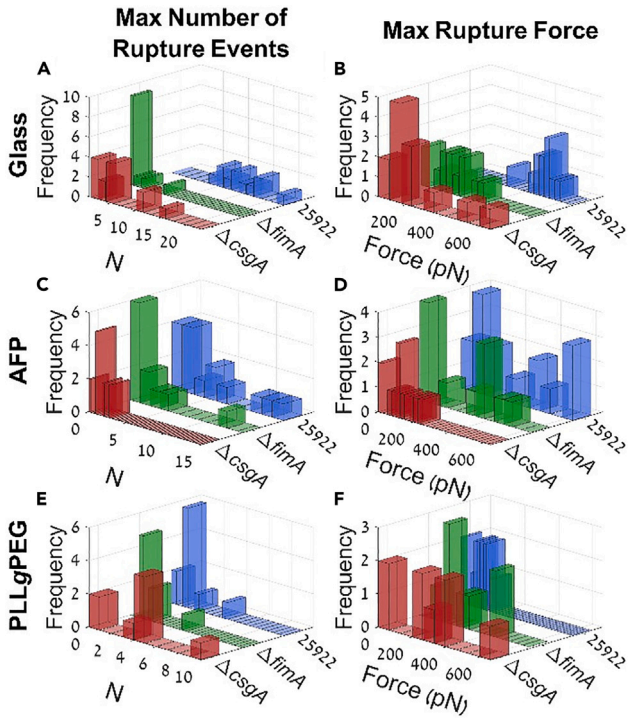

Figure 6. Quantitative analysis of the interaction measured for each bacterium of the WT, ΔfimA, and ΔcsgA strains with glass, AFP, or PLLgPEG

The data are presented as histograms, counting bacteria according to the maximal number of measured rupture events (in a single measurement) per cell, and the maximal rupture forces measured per cell. Histograms are shown for the number of rupture events (A) and the rupture force (B) on glass, the number of rupture events (C), and the rupture force (D) on AFP, the number of rupture events (E), and the rupture force on PLLgPEG (F).

DISCUSSION

In this study, we used FluidFM SCFS to investigate the adhesion of *E. coli* to glass, either bare or coated with an antifouling layer of AFP or PLLgPEG. Our results suggest that the interactions between *E. coli* and glass are mediated mainly by type 1 fimbriae. This is in accordance with previous reports.[11,50,51] Our results suggest that interactions with different antifouling surfaces have different mechanisms. The interaction with AFP seems to be more associated with curli amyloids. However, the interaction with PLLgPEG probably does not result from either type 1 or curli fimbriae adhesion.

Our results show that both antifouling surfaces impair the initial attachment of *E. coli*, by significantly reducing its probability of adhering to the surface. Moreover, even when bacteria do adhere to the antifouling surfaces, their interaction is significantly weaker, meaning that their ability to stay on the surface and resist cleaning procedures is hampered. Although the adhesive ability of most of the cell population is reduced, our analysis of single-cell adhesion potential indicates that some of the bacteria still possess the ability to adhere to the surface. This may lead to changes in the chemical environment, eventually damaging the antifouling properties and enabling biofilm formation.

These results shed light on the antifouling mechanisms of AFP and PLLgPEG. Furthermore, the development of new methodologies for studying bacteria at the single-cell level may offer new opportunities to enhance our understanding of these complex mechanisms. For instance, developing methodologies for a combination of SCFS with AFM imaging and advanced molecular biology methods for single-cell transcriptomic analysis[57,58] can greatly enhance our understanding of the attachment mechanism, which can help in developing the next generation of antifouling coatings.

Limitation of the study

This study focuses on the initial adhesion of bacteria to glass and glass coated with different antifouling layers. While it is possible to aspirate cells from suspension using FluidFM (in contrast to traditional AFM), it is difficult to determine whether more than one cell was aspirated when cells are abundant in the medium. For this reason, we focused on aspirating and measuring sessile cells. Even when working with well-adhered cells, any bacteria that remain suspended in the medium may interfere with the process of cell aspiration, as they may gather around the FluidFM probe as a result of applying under pressure. This in turn again compromises the single-cell probe preparation. Working only with bacteria already adhered to the substrate means that the probed cells are biased toward better adhesion, as poorly adhered cells were washed away during sample preparation. Furthermore, the SCFS experiments were performed in PBS rather than in a medium. These experimental conditions are not ideal for the bacteria, therefore to minimize contribution of stress, experimental sessions were kept relatively short (2–3 h long).

STAR★METHODS

Detailed methods are provided in the online version of this paper and include the following:

- KEY RESOURCES TABLE
- RESOURCE AVAILABILITY
  - Lead contact
  - Materials availability
  - Data and code availability
- METHOD DETAILS
  - Single-cell force spectroscopy (SCFS)
  - Substrate preparation
  - Substrate characterization
  - FluidFM probe preparation
  - Bacterial culture growth
  - Bacterial culture preparation on the substrate for SCFS measurements
  - SCFS measurements
  - FluidFM probe maintenance
  - SCFS data analysis
  - Bacterial AFM imaging
- QUANTIFICATION AND STATISTICAL ANALYSIS

SUPPLEMENTAL INFORMATION

Supplemental information can be found online at https://doi.org/10.1016/j.isci.2024.108803.

ACKNOWLEDGMENTS

This paper was prepared within the framework of the European Union's Horizon Europe Research and Innovation Programme under the Marie Sklodowska-Curie grant agreement no. 101072645(NanoReMedi; www.nanoremedi.eu). We thank Prof. S. Belkin's research group for supplying the K12 mutant strains and Mr. A. Vakahi for skillfully operating the FIB instrument.

AUTHOR CONTRIBUTIONS

T.D.A.: conceptualization, methodology, investigation, formal analysis, visualization, writing and editing. M.R.: supervision, conceptualization, methodology, writing and editing.

DECLARATION OF INTERESTS

The authors declare that they have no conflict of interest.

Received: July 10, 2023
Revised: October 29, 2023
Accepted: January 2, 2024
Published: January 6, 2024

REFERENCES

1. Costerton, J.W., Lewandowski, Z., Caldwell, D.E., Korber, D.R., and Lappin-Scott, H.M. (1995). Microbial biofilms. Annu. Rev. Microbiol. *49*, 711–745.
2. Hall-Stoodley, L., Costerton, J.W., and Stoodley, P. (2004). Bacterial biofilms: From the natural environment to infectious diseases. Nat. Rev. Microbiol. *2*, 95–108.
3. Nir, S., and Reches, M. (2016). Bio-inspired antifouling approaches: The quest towards non-toxic and non-biocidal materials. Curr. Opin. Biotechnol. *39*, 48–55.
4. Jacobsen, S.M., Stickler, D.J., Mobley, H.L.T., and Shirtliff, M.E. (2008). Complicated catheter-associated urinary tract infections due to *escherichia coli* and *proteus mirabilis*. Clin. Microbiol. Rev. *21*, 26–59.
5. Beloin, C., Roux, A., and Ghigo, J.-M. (2008). *Escherichia coli* biofilms. In Bacterial biofilms, T. Romeo, ed. (Springer).
6. Andreasen, M., Meisl, G., Taylor, J.D., Michaels, T.C.T., Levin, A., Otzen, D.E., Chapman, M.R., Dobson, C.M., Matthews, S.J., and Knowles, T.P.J. (2019). Physical determinants of amyloid assembly in biofilm formation. mBio *10*, e02279-18–e02218.
7. Fronzes, R., Remaut, H., and Waksman, G. (2008). Architectures and biogenesis of non-flagellar protein appendages in gram-negative bacteria. EMBO J. *27*, 2271–2280.
8. Krogfelt, K.A., Bergmans, H., and Klemm, P. (1990). Direct evidence that the fimh protein is the mannose-specific adhesin of *escherichia coli* type 1 fimbriae. Infect. Immun. *58*, 1995–1998.
9. Sheikh, A., Rashu, R., Begum, Y.A., Kuhlman, F.M., Ciorba, M.A., Hultgren, S.J., Qadri, F., and Fleckenstein, J.M. (2017). Highly conserved type 1 pili promote enterotoxigenic *e. Coli* pathogen-host interactions. PLoS Neglected Trop. Dis. *11*, e0005586.
10. Pratt, L.A., and Kolter, R. (1998). Genetic analysis of *escherichia coli* biofilm formation: Roles of flagella, motility, chemotaxis and type i pili. Mol. Microbiol. *30*, 285–293.
11. Cookson, A.L., Cooley, W.A., and Woodward, M.J. (2002). The role of type 1 and curli fimbriae of shiga toxin-producing *escherichia coli* in adherence to abiotic surfaces. Int. J. Med. Microbiol. *292*, 195–205.
12. Reisner, A., Maierl, M., Jörger, M., Krause, R., Berger, D., Haid, A., Tesic, D., and Zechner,

E.L. (2014). Type 1 fimbriae contribute to catheter-associated urinary tract infections caused by *escherichia coli*. J. Bacteriol. *196*, 931–939.
13. Chapman, M.R., Robinson, L.S., Pinkner, J.S., Roth, R., Heuser, J., Hammar, M., Normark, S., and Hultgren, S.J. (2002). Role of *escherichia coli* curli operons in directing amyloid fiber formation. Science *295*, 851–855.
14. Elpers, L., and Hensel, M. (2020). Expression and functional characterization of various chaperon-usher fimbriae, curli fimbriae, and type 4 pili of enterohemorrhagic *escherichia coli* o157: H7 sakai. Front. Microbiol. *11*, 378.
15. Cohen, N., Zhou, H., Hay, A.G., and Radian, A. (2019). Curli production enhances clay-*e. Coli* aggregation and sedimentation. Colloids Surf. B Biointerfaces *182*, 110361.
16. Mao, X., Li, K., Liu, M., Wang, X., Zhao, T., An, B., Cui, M., Li, Y., Pu, J., Li, J., et al. (2019). Directing curli polymerization with DNA origami nucleators. Nat. Commun. *10*, 1395.
17. Jiang, C., Wang, G., Hein, R., Liu, N., Luo, X., and Davis, J.J. (2020). Antifouling strategies for selective in vitro and in vivo sensing. Chem. Rev. *120*, 3852–3889.
18. Prime, K.L., and Whitesides, G.M. (1993). Adsorption of proteins onto surfaces containing end-attached oligo(ethylene oxide): A model system using self-assembled monolayers. J. Am. Chem. Soc. *115*, 10714–10721.
19. Li, B., Jain, P., Ma, J., Smith, J.K., Yuan, Z., Hung, H.C., He, Y., Lin, X., Wu, K., Pfaendtner, J., and Jiang, S. (2019). Trimethylamine n-oxide-derived zwitterionic polymers: A new class of ultralow fouling bioinspired materials. Sci. Adv. *5*, eaaw9562.
20. Hui, N., Sun, X., Niu, S., and Luo, X. (2017). Pegylated polyaniline nanofibers: Antifouling and conducting biomaterial for electrochemical DNA sensing. ACS Appl. Mater. Interfaces *9*, 2914–2923.
21. Wong, T.-S., Kang, S.H., Tang, S.K.Y., Smythe, E.J., Hatton, B.D., Grinthal, A., and Aizenberg, J. (2011). Bioinspired self-repairing slippery surfaces with pressure-stable omniphobicity. Nature *477*, 443–447.
22. Tong, Z., Song, L., Chen, S., Hu, J., Hou, Y., Liu, Q., Ren, Y., Zhan, X., and Zhang, Q. (2022). Hagfish-inspired smart slips marine antifouling coating based on supramolecular: Lubrication modes responsively switching and self-healing properties. Adv. Funct. Mater. *32*, 2201290.
23. Tesler, A.B., Kim, P., Kolle, S., Howell, C., Ahanotu, O., and Aizenberg, J. (2015). Extremely durable biofouling-resistant metallic surfaces based on electrodeposited nanoporous tungstite films on steel. Nat. Commun. *6*, 8649.
24. Yuran, S., Dolid, A., and Reches, M. (2018). Resisting bacteria and attracting cells: Spontaneous formation of a bifunctional peptide-based coating by on-surface assembly approach. ACS Biomater. Sci. Eng. *4*, 4051–4061.
25. Ham, H.O., Park, S.H., Kurutz, J.W., Szleifer, I.G., and Messersmith, P.B. (2013). Antifouling glycocalyx-mimetic peptoids. J. Am. Chem. Soc. *135*, 13015–13022.
26. Gu, S., Shi, X.-M., Zhang, D., Fan, G.-C., and Luo, X. (2021). Peptide-based photocathodic biosensors: Integrating a recognition peptide with an antifouling peptide. Anal. Chem. *93*, 2706–2712.
27. Chelmowski, R., Köster, S.D., Kerstan, A., Prekelt, A., Grunwald, C., Winkler, T., Metzler-Nolte, N., Terfort, A., and Wöll, C. (2008). Peptide-based sams that resist the adsorption of proteins. J. Am. Chem. Soc. *130*, 14952–14953.
28. Viljoen, A., Mathelié-Guinlet, M., Ray, A., Strohmeyer, N., Oh, Y.J., Hinterdorfer, P., Müller, D.J., Alsteens, D., and Dufrêne, Y.F. (2021). Force spectroscopy of single cells using atomic force microscopy. Nat. Rev. Methods Primers *1*, 63.
29. Binnig, G., Quate, C.F., and Gerber, C. (1986). Atomic force microscope. Phys. Rev. Lett. *56*, 930–933.
30. Sullan, R.M.A., Beaussart, A., Tripathi, P., Derclaye, S., El-Kirat-Chatel, S., Li, J.K., Schneider, Y.J., Vanderleyden, J., Lebeer, S., and Dufrêne, Y.F. (2014). Single-cell force spectroscopy of pili-mediated adhesion. Nanoscale *6*, 1134–1143.
31. Khan, N., Aslan, H., Büttner, H., Rohde, H., Golbek, T.W., Roeters, S.J., Woutersen, S., Weidner, T., and Meyer, R.L. (2022). The giant staphylococcal protein embp facilitates colonization of surfaces through velcro-like attachment to fibrillated fibronectin. Elife *11*, e76164.
32. Rodriguez-Emmenegger, C., Janel, S., de los Santos Pereira, A., Bruns, M., and Lafont, F. (2015). Quantifying bacterial adhesion on antifouling polymer brushes via single-cell force spectroscopy. Polym. Chem. *6*, 5740–5751.
33. Duanis-Assaf, D., Duanis-Assaf, T., Zeng, G., Meyer, R.L., Reches, M., Steinberg, D., and Shemesh, M. (2018). Cell wall associated protein tasa provides an initial binding component to extracellular polysaccharides in dual-species biofilm. Sci. Rep. *8*, 9350.
34. Zeng, G., Müller, T., and Meyer, R.L. (2014). Single-cell force spectroscopy of bacteria enabled by naturally derived proteins. Langmuir *30*, 4019–4025.
35. Meister, A., Gabi, M., Behr, P., Studer, P., Vörös, J., Niedermann, P., Bitterli, J., Polesel-Maris, J., Liley, M., Heinzelmann, H., and Zambelli, T. (2009). Fluidfm: Combining atomic force microscopy and nanofluidics in a universal liquid delivery system for single cell applications and beyond. Nano Lett. *9*, 2501–2507.
36. Potthoff, E., Ossola, D., Zambelli, T., and Vorholt, J.A. (2015). Bacterial adhesion force quantification by fluidic force microscopy. Nanoscale *7*, 4070–4079.
37. Hofherr, L., Müller-Renno, C., and Ziegler, C. (2020). Fluidfm as a tool to study adhesion forces of bacteria - optimization of parameters and comparison to conventional bacterial probe scanning force spectroscopy. PLoS One *15*, e0227395.
38. Maan, A.M.C., Hofman, A.H., de Vos, W.M., and Kamperman, M. (2020). Recent developments and practical feasibility of polymer-based antifouling coatings. Adv. Funct. Mater. *30*, 2000936.
39. Maity, S., Nir, S., Zada, T., and Reches, M. (2014). Self-assembly of a tripeptide into a functional coating that resists fouling. Chem. Commun. *50*, 11154–11157.
40. Hardelauf, H., Waide, S., Sisnaiske, J., Jacob, P., Hausherr, V., Schöbel, N., Janasek, D., van Thriel, C., and West, J. (2014). Micropatterning neuronal networks. Analyst *139*, 3256–3264.
41. Dufrêne, Y.F. (2015). Sticky microbes: Forces in microbial cell adhesion. Trends Microbiol. *23*, 376–382.
42. Wilms, D., Schröer, F., Paul, T.J., and Schmidt, S. (2020). Switchable adhesion of *e. Coli* to thermosensitive carbohydrate-presenting microgel layers: A single-cell force spectroscopy study. Langmuir *36*, 12555–12562.
43. Viljoen, A., Mignolet, J., Viela, F., Mathelié-Guinlet, M., and Dufrêne, Y.F. (2020). How microbes use force to control adhesion. J. Bacteriol. *202*, e00125-20–e00120.
44. Beaussart, A., Abellán-Flos, M., El-Kirat-Chatel, S., Vincent, S.P., and Dufrêne, Y.F. (2016). Force nanoscopy as a versatile platform for quantifying the activity of antiadhesion compounds targeting bacterial pathogens. Nano Lett. *16*, 1299–1307.
45. Beaussart, A., Baker, A.E., Kuchma, S.L., El-Kirat-Chatel, S., O'Toole, G.A., and Dufrêne, Y.F. (2014). Nanoscale adhesion forces of *pseudomonas aeruginosa* type iv pili. ACS Nano *8*, 10723–10733.
46. Zuttion, F., Ligeour, C., Vidal, O., Wälte, M., Morvan, F., Vidal, S., Vasseur, J.J., Chevolot, Y., Phaner-Goutorbe, M., and Schillers, H. (2018). The anti-adhesive effect of glycoclusters on *pseudomonas aeruginosa* bacteria adhesion to epithelial cells studied by afm single cell force spectroscopy. Nanoscale *10*, 12771–12778.
47. Baba, T., Ara, T., Hasegawa, M., Takai, Y., Okumura, Y., Baba, M., Datsenko, K.A., Tomita, M., Wanner, B.L., and Mori, H. (2006). Construction of *escherichia coli* k-12 in-frame, single-gene knockout mutants: The keio collection. Mol. Syst. Biol. *2*, 2006.
48. Feng, G., Cheng, Y., Wang, S.Y., Hsu, L.C., Feliz, Y., Borca-Tasciuc, D.A., Worobo, R.W., and Moraru, C.I. (2014). Alumina surfaces with nanoscale topography reduce attachment and biofilm formation by *escherichia coli* and *listeria* spp. Biofouling *30*, 1253–1268.
49. Rubin, M. (2021). When to adjust alpha during multiple testing: A consideration of disjunction, conjunction, and individual testing. Synthese *199*, 10969–11000.
50. Wong, K.K.W., Olsson, A.L.J., Asadishad, B., van der Bruggen, B., and Tufenkji, N. (2017). Role of cell appendages in initial attachment and stability of *e. Coli* on silica monitored by nondestructive tirf microscopy. Langmuir *33*, 4066–4075.
51. McLay, R.B., Nguyen, H.N., Jaimes-Lizcano, Y.A., Dewangan, N.K., Alexandrova, S., Rodrigues, D.F., Cirino, P.C., and Conrad, J.C. (2018). Level of fimbriation alters the adhesion of *escherichia coli* bacteria to interfaces. Langmuir *34*, 1133–1142.
52. Wang, X., and Chapman, M.R. (2008). Sequence determinants of bacterial amyloid formation. *J.* Mol. Biol. *380*, 570–580.
53. Gazit, E. (2002). A possible role for π-stacking in the self-assembly of amyloid fibrils. Faseb. J. *16*, 77–83.
54. Zeng, G., Ogaki, R., and Meyer, R.L. (2015). Non-proteinaceous bacterial adhesins challenge the antifouling properties of polymer brush coatings. Acta Biomater. *24*, 64–73.
55. Ostuni, E., Chapman, R.G., Holmlin, R.E., Takayama, S., and Whitesides, G.M. (2001). A survey of structure−property relationships of surfaces that resist the adsorption of protein. Langmuir *17*, 5605–5620.
56. Altschuler, S.J., and Wu, L.F. (2010). Cellular heterogeneity: Do differences make a difference? Cell *141*, 559–563.
57. Tang, F., Lao, K., and Surani, M.A. (2011). Development and applications of single-cell transcriptome analysis. Nat. Methods *8*, S6–S11.

58. Taniguchi, Y., Choi, P.J., Li, G.W., Chen, H., Babu, M., Hearn, J., Emili, A., and Xie, X.S. (2010). Quantifying E. *coli* proteome and transcriptome with single-molecule sensitivity in single cells. Science *329*, 533–538.
59. Duanis-Assaf, T., Razvag, Y., and Reches, M. (2019). Forsdat: An automated platform for analyzing force spectroscopy measurements. Anal. Methods *11*, 4709–4718.
60. Friedlander, A., Nir, S., Reches, M., and Shemesh, M. (2019). Preventing biofilm formation by dairy-associated bacteria using peptide-coated surfaces. Front. Microbiol. *10*, 1405.
61. Berent, K., and Faryna, M. (2012). High resolution EBSD/SEM analysis of plzt ferroelectric crystals in low vacuum conditions - a few practical remarks. Solid State Phenom. *186*, 62–65.
62. Saha, P., Duanis-Assaf, T., and Reches, M. (2020). Fundamentals and applications of fluidfm technology in single-cell studies. Adv. Mater. Interfac. *7*, 2001115.
63. Dörig, P., Stiefel, P., Behr, P., Sarajlic, E., Bijl, D., Gabi, M., Vörös, J., Vorholt, J.A., and Zambelli, T. (2010). Force-controlled spatial manipulation of viable mammalian cells and micro-organisms by means of fluidFm technology. Appl. Phys. Lett. *97*, 023701.
64. Dörig, P., Ossola, D., Truong, A.M., Graf, M., Stauffer, F., Vörös, J., and Zambelli, T. (2013). Exchangeable colloidal AFM probes for the quantification of irreversible and long-term interactions. Biophys. J. *105*, 463–472.
65. Shemer, B., Shpigel, E., Glozman, A., Yagur-Kroll, S., Kabessa, Y., Agranat, A.J., and Belkin, S. (2020). Genome-wide gene-deletion screening identifies mutations that significantly enhance explosives vapor detection by a microbial sensor. N. Biotech. *59*, 65–73.
66. Reches, M., and Duanis-Assaf, T. (2023). In situ measurements of cell mechanical properties using force spectroscopy. In *Mechanobiology*) (Springer).
67. Sader, J.E., Chon, J.W.M., and Mulvaney, P. (1999). Calibration of rectangular atomic force microscope cantilevers. Rev. Sci. Instrum. *70*, 3967–3969.
68. Zeng, G., Vad, B.S., Dueholm, M.S., Christiansen, G., Nilsson, M., Tolker-Nielsen, T., Nielsen, P.H., Meyer, R.L., and Otzen, D.E. (2015). Functional bacterial amyloid increases *pseudomonas* biofilm hydrophobicity and stiffness. Front. Microbiol. *6*, 1099.

STAR★METHODS

KEY RESOURCES TABLE

REAGENT or RESOURCE	SOURCE	IDENTIFIER
Bacterial and virus strains		
E. coli	ATCC	ATCC 25922
E. coli ΔcsgA	Keio collection,[47] kindly supplied by Belkin research lab, Hebrew University	*ΔcsgA*
E. coli ΔfimA	Keio collection,[47] kindly supplied by Belkin research lab, Hebrew University	*ΔfimA*
Chemicals, peptides, and recombinant proteins		
Antifouling peptide (AFP)	CSBio, USA	DOPA-Phe(4F)-Phe(4F)-OMe
PLL*g*PEG	Surface Solution SuSoS AG, Switzerland	PLL(20)-g[3.5]-PEG(2)
Software and algorithms		
Matlab	Mathworks	Matlab2021-a
ForSDAT version 1.2	Duanis-Assaf et al.[59]	https://github.com/TaDuAs/ForSDAT/releases/tag/1.2.0
Other		
FluidFM probes	Cytosurge AG, Switzerland	MAT FluidFM Nanopipette for Bruker & JPK AFMs
AFM	Bruker, JPK BIOAFM	NanoWizard III
FluidFM	Cytosurge AG, Switzerland	FluidFM ADD-ON for Bruker & JPK AFMs
Focused ion beam (FIB)	FEI, USA	Helios NanoLab 460F1
AFM probes for imaging	Team Nanotec, Germany	Aspire CFM probe

RESOURCE AVAILABILITY

Lead contact

Further information and requests for resources and reagents should be directed to and will be fulfilled by the lead contact, Meital Reches (meital.reches@mail.huji.ac.il)

Materials availability

This study did not generate new unique reagents.

Data and code availability

All data reported in this paper will be shared by the lead contact upon request.
All the data were analyzed using ForSDAT version 1.2.0.
The computer codes are available at https://github.com/TaDuAs/ForSDAT/releases/tag/1.2.0. This version includes two new types of raw data analyzers, max adhesion force and detachment work analyzers. Moreover, better archiving of analyzed data is also present to allow faster analysis of full data sets between sessions.

METHOD DETAILS

Single-cell force spectroscopy (SCFS)

To measure the initial attachment of single bacterial cells with a substrate of interest, single-cell force spectroscopy (SCFS) was performed using a fluid force microscope (FluidFM; Cytosurge FluidFM integrated Nano Wizard III, JPK instruments, Germany and Cytosurge AG, Switzerland), mounted on an inverted optical microscope (Eclipse Ti-E, Nikon Instruments, USA).

Substrate preparation

Glass slides were sonicated in 70% ethanol (Gadot group, Israel) for 15 min, then washed with 96% ethanol (Gadot group, Israel), ultrapure water (Milli-Q, Merck, USA), and dried with a flow of nitrogen.

Glass surfaces coated with the antifouling peptide (AFP) were prepared as previously described.[39,60] Briefly, ethanol-cleaned glass slides were covered with a drop of 500 μL solution, 0.5 mg/mL DOPA-Phe(4F)-Phe(4F)-OMe (CSBio, USA) in dehydrated ethanol (Bio-Lab, Israel),

overnight at room temperature. The substrates were then thoroughly rinsed with ethanol and dried with a nitrogen flow. The substrates were kept in a vacuumed desiccator until use.

Glass surfaces coated with a commercially available antifouling agent, polylysine (20 kDa) grafted with poly-ethylene glycol (PEG) (2 kDa) (PLL*g*PEG) (Surface Solution SuSoS AG, Switzerland), were prepared according to the manufacturer's protocol. Briefly, ethanol-cleaned glass slides were treated with O_2 plasma (Atto, Diener Electronic, Germany) for 2 min. Next, the substrates were immediately covered with 200 μL solution of 0.5 mg/mL PLL*g*PEG in ultrapure water and incubated for 1 h at room temperature. The substrates were then rigorously washed with ultrapure water, dried with a nitrogen flow, and kept under argon, in a vacuumed desiccator until use. A portion of the slide was left untreated, to allow the adhesion of bacteria during the incubation period before each experiment.

Substrate characterization

The substrates were characterized by water contact angle using a Theta Lite optical tensiometer (Attension, Finland). The measurements were performed at three different locations and the reported values were averaged.

The substrates' elementary composition was analyzed by energy-dispersive X-ray spectroscopy (EDS) using an Apreo 2S scanning electron microscope (Thermo Scientific, USA), equipped with an UltraDry EDS detector (Thermo Scientific, USA). The measurements were performed on an area of $26 \cdot 10^3$ μm^2, over a time frame of 60 s, at a voltage of 5 kV, and with a current of 0.2 nA. To avoid the need to coat the surface with a conductive layer, which affects the surface elemental composition, the measurements were carried out in a low vacuum (0.38 Torr), which assists in surface discharge.[61]

FluidFM probe preparation

To fabricate a FluidFM probe with an orifice suitable to trap an individual bacterial cell, we used a focused ion beam (FIB) instrument to mill the apex of the tip of a FluidFM Nanopipette with an aperture size of 300 nm, and a nominal cantilever spring constant of 0.6 N/m (Cytosurge AG, Switzerland).[62] We used the previously described procedure[36] with minor changes. First, we coated the FluidFM probe with a thin conductive layer of titanium (7 nm), to discharge the electron/ion beams in the FIB, using electron beam evaporation (TFDS-141E, VST) at a rate of 1 Å/s. Prior to the Ti coating, the probes were treated by O_2 plasma for 30 s to remove atmospheric hydrocarbons without wetting the probes. Next, the coated probes were milled using a DualBeam FIB system (Helios NanoLab 460F1, FEI, USA) until an aperture size of approximately 800 nm was achieved.

After the probe was milled to the desired crevice size, an antifouling coating was applied to the probe. This anti-adhesive layer serves a dual purpose. First, it prevents the probed bacterium from unintentionally attaching irreversibly to the tip. Second, it prevents other cells, suspended in the medium, as well as any biological residues produced by the bacteria from adhering to the probe. We used the previously reported poly(L-lysine) grafted with polyethylene glycol (PLL*g*PEG).[63,64] Using this approach, a single probe can be used repeatedly for measuring the adhesive interactions of many single bacteria. Briefly, the probes were treated with O_2 plasma (Atto, Diener Electronic, Germany) for 30 s. The probes were then immediately treated with a solution of 0.5 mg/mL PLL*g*PEG in ultrapure water. To coat the probe inside and outside it, the probe liquid reservoir was loaded with 10 μL of the PLL*g*PEG solution. A pressure of 1000 mbar was applied to generate a flow of PLL*g*PEG solution through the microfluidic channel inside the cantilever. The probe was loaded onto the FluidFM instrument and monitored using an optical microscope. When a drop of liquid visibly formed outside the probe aperture, an extra 200 μL PLL*g*PEG solution was applied to immerse the entire probe surface. The probe was incubated for 1 h to allow the PLL to adhere permanently to the probe surface. Next, the probe was washed repeatedly with ultrapure water to remove any excess PLL*g*PEG solution, to prevent it from interfering with the measurements. The solution in the liquid reservoir was replaced with ultrapure water, and an overpressure of 1000 mbar was applied for 10 min, to remove excess PLL*g*PEG solution from the microfluidic channel inside the cantilever.

Bacterial culture growth

E. coli strains ATCC 25922, K-12 *ΔcsgA*, and K-12 *ΔfimA* cultures were routinely grown on LB (Difco, BD, USA) agar (Sigma-Aldrich, USA) plates. The K-12 mutant strains were grown on plates supplemented with 50 μg mL^{-1} kanamycin sulfate (Fisher Bioreagents, USA).[65] For *E. coli* 25922 starters, a fresh colony was suspended in 3 mL LB broth and grown at 37°C and 120 rpm for 3.5 h. For K-12 mutant strain starters, a fresh colony was suspended in 10 mL LB broth supplemented with 50 μg mL^{-1} kanamycin sulfate,[65] and grown at 37°C and 120 rpm overnight. The starters were then washed three times with phosphate-buffered saline (PBS) by centrifugation (5000 rpm, 3 min), resuspended in PBS, and then diluted to a final OD (600nm) of 0.0125.

Bacterial culture preparation on the substrate for SCFS measurements

A drop of 40 μL of diluted bacterial suspension was applied on the substrate of interest and was left for 30 min at room temperature, to allow the bacteria to attach to the surface. To wash off any suspended bacteria that may interfere with the measurement, the liquid was then removed with a pipette while adding more PBS using a second pipette to prevent the bacteria from drying.[66]

SCFS measurements

The FluidFM probe was calibrated for each SCFS session before introducing the bacteria sample. The FluidFM probe was placed above a glass slide in PBS. Next, calibration was performed using the Sader method[67] built into the AFM software (contactless calibration).

A substrate incubated with the bacterial suspension was placed on the microscope stage. The FluidFM probe was optically aligned above a single bacterium. Then, the probe was approached and a negative pressure of 800 mbar was applied to aspirate the cell. To minimize the chance to aspirate several cells, the bacteria were chosen with minimal surrounding bacterial cells. Alternatively, the surrounding area was cleared of weakly attached bacteria by applying a high positive pressure (1000 mbar) and moving the FluidFM probe above the cells at a small circle around the bacterium of interest. If this method is used, caution must be taken to prevent the disturbance of the bacterium of interest. Moreover, this method is less viable when the cells strongly adhere to the substrate. Aspiration was confirmed visually by ensuring that the bacterium was removed when the probe was set aside.

SCFS was performed immediately once a bacterium was aspirated. These measurements were performed using contact mode force spectroscopy. The bacterial probe was positioned next to the substrate up to a setpoint of 10 nN. The probe was in contact for 10 s to allow bacterial adhesion. Next, the probe was retracted at a constant speed of 2 $\mu m\ s^{-1}$ up to a distance of 2.5 μm to ensure complete detachment between the bacterial probe and the substrate. With each bacterium, 25 force vs. distance curves were recorded, on an area of 100 μ^2. The bacterium was then discarded by applying a positive pressure of 1000 mbar, and the clean probe was then reused to aspirate another bacterium.

To minimize the variability resulting from different exposure times of the bacteria to the unfavorable conditions during measurements, SCFS sessions were kept relatively short. Each SCFS session was performed for up to 3 h.

FluidFM probe maintenance

After each measurement, the probe was repeatedly washed with ultrapure water from inside and outside, to remove salt residues from the buffer medium. This was done by replacing the water in the liquid reservoir with fresh ultrapure water, and applying over-pressure, and by immersing the probe three times in fresh ultrapure water. The probes were then stored with the cantilever facing downwards in an antibiotic-antimycotic solution (Sigma-Aldrich, USA), inside a 24-well plate. Immersion in this solution serves two purposes: it prevents the probes' internal microfluidic channel from drying, which damages its function, and it prevents the growth of microorganisms. Finally, the water in the liquid reservoir was replaced by fresh ultrapure water.

When the probes were reused, prior to each experiment, the probe was washed with ultrapure water from inside and outside as described above, to wash off all traces of the antibiotic-antimycotic solution. This minimizes the risk of the antibiotics inducing stress in the bacteria, as well as compromising their viability.

SCFS data analysis

The data were analyzed using ForSDAT[59] version 1.2.0 (all the code is available to download from https://github.com/TaDuAs/ForSDAT/releases/tag/1.2.0) in manual supervision mode. The baseline was aligned using the force distribution method (the histogram method).[59] The contact point was aligned, and the curves were converted to force vs. extension curves. The rupture events were detected and evaluated using the first derivative, and the maximum adhesion force and detachment work were calculated by the minimal force on the aligned curve and the area under the curve, respectively; both were calculated according to the distance of the last detected rupture event. The curves were pretreated with Fourier series to eliminate oscillation artifacts as needed. For reference, force curves featuring 2, 4 and 6 detected rupture events are shown in Figure S3. To evaluate the magnitude of individual rupture events between the different groups, we chose to compare average values, calculated as arithmetic means to avoid introducing bias as not all groups seem to follow normal distribution well (Figure S4).

Bacterial AFM imaging

Imaging of the bacterial cell surface was performed using a NanoWizard III AFM (JPK instruments, Germany) mounted on an inverted optical microscope (Eclipse Ti-E, Nikon Instruments, USA). To better immobilize the cells as well as any of their extracellular features, such as appendages, while images were acquired, imaging was performed under dry conditions. This approach reduced any unwanted movement and sliding artifacts while imaging. We used a previously reported procedure with minor changes.[68] Briefly, after washing the starter cultures with PBS, the cultures were washed again with ultrapure water to remove salts and then resuspended in ultrapure water. To minimize damage to the cells due to osmotic pressure, a drop of 20 μL bacterial suspension was immediately placed on a freshly cleaved mica surface and left to dry. After having been dried, the samples were placed on the microscope stage. The AFM was mounted with an Aspire CFM probe (Team Nanotec, Germany). Finally, the probe was optically aligned over single cells, and images were acquired in tapping mode.

QUANTIFICATION AND STATISTICAL ANALYSIS

For each pair of bacterial strain and substrate, at least 8 cells were probed (the exact numbers are reported in Table S3). These cells were taken from at least two independently grown cultures. For each cell, a total of 25 force curves were acquired. Statistical analysis was performed using one-way ANOVA, followed by a post hoc Bonferroni test with an overall confidence level of $\alpha = 0.05$, unless stated otherwise. When the statistical analysis was performed on individual groups, a two-tailed t-test was used with a confidence level of $\alpha = 0.05$.